Shear-induced conductor-insulator transition in melt-mixed polypropylene-carbon nanotube dispersions

J. Obrzut,[1,*,†] J. F. Douglas,[1,*,‡] S. B. Kharchenko,[2] and K. B. Migler[1]
[1]*Polymers Division, National Institute of Standards and Technology, Gaithersburg, Maryland 20899, USA*
[2]*Masco Corporation, Taylor, Michigan 48180, USA*
(Received 17 May 2007; revised manuscript received 11 September 2007; published 15 November 2007)

The blending of carbon nanotubes (CNTs) into polymer matrices leads to intrinsically nonequilibrium materials whose properties can depend strongly on flow history. We have constructed a rheodielectric spectrometer that allows for the simultaneous *in situ* measurement of both the electrical conductivity $\sigma(\omega)$ and dielectric constant $\varepsilon(\omega)$ as a function of frequency ω, as well as basic rheological properties (viscosity, normal stresses), as part of an effort to better characterize how flow alters the properties of these complex fluids. Measurements of σ indicate a conductor-insulator transition in melt-mixed dispersions of multiwall CNTs in polypropylene over a narrow range of CNT concentrations that is reasonably described by the generalized effective medium theory. A conductor-insulator transition in σ can also be induced by shearing the fluid at a fixed CNT concentration ϕ near, but above, the zero shear CNT conductivity percolation threshold ϕ_c. We find that the shear-induced conductor-insulator transition has its origin in the shear-rate dependence of ϕ_c, which conforms well to a model introduced to describe this effect. Surprisingly, σ of these nonequilibrium materials fully recovers at these elevated temperatures upon cessation of flow. We also find that the frequency dependence of $\sigma(\omega)$ follows a "universal" scaling relation observed for many other disordered materials.

DOI: 10.1103/PhysRevB.76.195420 PACS number(s): 73.63.Fg, 72.80.Tm, 83.80.Ab

INTRODUCTION

There is a growing interest in adding small concentrations of carbon nanotubes (CNTs) to plastics to impart multifunctional capabilities to the materials, including electrical[1–6] and thermal[7–10] conductivities as well as changes in the bulk and shear modulus.[7,11,12] Perhaps the most significant applications to date involve conductivity enhancements in numerous applications where conductive polymeric materials are required. Specifically, CNT dispersions have led to applications in sensors,[13,14] electrospraying of car parts, and in the semiconductor and automotive industries relating to the dissipation of unwanted charge.[2,15]

The large changes of the properties of nanocomposites of CNT and polymer materials are typically discussed in terms of the percolation theory. Most commonly, CNTs are isolated from each other at low concentrations. The composite is then an insulator since the conductivity of the polymer matrix is taken to be negligibly small, but a "percolating" network of particles forms at higher concentrations as the randomly positioned and oriented particles begin to "overlap." Geometrical percolation theory also requires that the particles are either perfectly conducting (or insulating when insulating particles are considered) or that they can freely overlap (no excluded volume interactions), which leads to a divergence of the conductivity in the case of "superconducting" inclusions at a well-defined "geometrical percolation threshold." In reality, the matrix polymer has a nonvanishing conductivity and the conductivity of the carbon nanocomposite tends to approach a limiting finite value at high CNT loadings, features that cannot be described by the geometrical percolation theory. The conductivity transition in this type of material is thus not really a purely geometrical phenomenon. The application of an oscillating electric field to a relatively insulating matrix material with conducting inclusions at fixed frequency distorts the charge distribution on these conducting particles and induces a strong dipole moment on the particle interaction that reacts upon the applied external electric field.[16,17] These large dipolar interaction fields generated by the particles begin to overlap beyond a critical particle concentration that depends on the particle shape and the interfacial properties of the particles, resulting in a *screening transition* where the particle configuration as a whole responds like a single collective body of relatively high conductivity so that charges can then be displaced over large distances by the applied field. We term the "critical concentration" where this electrodynamic transition occurs a "conductivity percolation threshold" ϕ_c, by analogy with geometrical percolation theory, but it should be appreciated that there is no simple relation between the percolation threshold calculated from the continuum theory of the dielectric properties of heterogeneous materials and the threshold geometrical percolation theory in either on-lattice or off-lattice versions.[18]

Below, we use the generalized effective medium (GEM) theory[19,20] to describe the dependence of the conductivity of our polymer dispersions on CNT concentration under both quiescent and steady shear conditions. This model involves an "amalgamation" of effective medium theory, a mean field theory generalizing the original continuum Maxwell approach to describe the properties of mixtures, with ideas drawn from percolation theory that address the formation of clusters within the material as the concentration increases. The advantage of this approach is that it allows a description of the crossover between the high and low conductivity states that is characteristic of these and many other composite materials, while percolation theory descriptions restrict attention to concentrations near ϕ_c where large changes in conductivity and in other properties occur. While GEM has its theoretical shortcomings, we find that we can fit our data

well to this model over a wide range of conditions, allowing an estimation of the conductivity in the high and low concentration limits and for a range of shear rates, and this model also allows reliable estimates of the conductivity percolation threshold as a function of shear rate.

The diffusion of carbon nanotubes in a viscous polymer matrix is rather slow,[7] if not negligible, and the CNT configurations do not generally correspond to equilibrium conformations as one might encounter in solutions. Under such nonequilibrium conditions, the aggregation of the tubes arising from direct nanotube-nanotube attractive interactions and topological interactions under fluid flow are the crucial determinant of the properties of the resulting dispersion. These dispersions can thus exhibit properties that strongly depend on the flow history to which they have been subjected, but little is known quantitatively about this general phenomenon. In this paper, we thus attempt to quantify these relationships by developing a method to measure conductivity in well-defined flow fields and by observing the dependence of conductivity on shear rate, composition, and annealing time. We can also expect the carbon nanotubes to become substantially deformed under flow conditions, so these objects are somewhat akin to wound up "springs" that store elastic deformation energy under flow. The release of these stresses in a quenched polymer nanocomposite material over time can be expected to affect the mechanical properties of these materials, substantially leading to appreciable property evolutions in the material over time that could affect the susceptibility of the material to failure (a relevant concern for aerospace applications where material failure can have catastrophic consequences). To obtain an initial insight into this general phenomenon, we performed stopped flow measurements on our carbon annotate filled polymer melts and found that σ indeed evolves substantially over time. A similar phenomenon can be expected at low temperatures, except that the time constant for this aging phenomenon should be much longer.

Previous studies of conductivity in CNT dispersions have established the importance of the flow processing conditions[15,21,22] on nanocomposite properties. Under typical processing conditions used to prepare the materials, the flow is time dependent and complex (mixtures of different types, i.e., shear and extensional). In that study, we focused mainly on the rheological properties of CNT-polypropylene (PP) dispersions[7] where the CNT mass fraction was varied from 0.0025 to 0.15. In this previous work, we also briefly considered the effects of shear on conductivity in comparison with the observed rheological property changes. These materials exhibited unusual rheological and processing characteristics including shear thinning, *negative* normal stress differences, and a suppression of die swell. In the steady shear measurements, we utilized a flow cell where we averaged the conductivity over a wide range of shear rates and did not find a sharp conductivity transition with shear.

In this paper, we investigate these materials using a rheodielectric spectrometer that we have constructed to measure the alternating current (ac) conductivity during shear flow at well-defined shear rates. We seek to determine the conditions under which these materials exhibit a *maximum sensitivity* to perturbations, and we thus focused on the concentration regime near the conductivity percolation threshold where the tenuous conducting CNT network is the most fragile. We found a sharply defined conductor-insulator transition as a function of shear rate and CNT fraction, and we quantified the recovery of the material conductivity upon the cessation of flow.

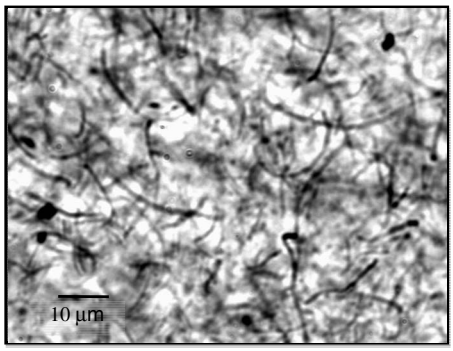

FIG. 1. Confocal optical image of CNT-PP melt at CNT concentration $x_m=0.01$.

MATERIALS AND MEASUREMENTS

Details of the synthesis procedure of the CNTs and their dispersion in the PP matrix of the present work have been described in previous papers,[23,24] so we only describe essential aspects of the CNT formation and their dispersion in PP. The CNTs used in our study are multiwalled, grown in a chemical vapor deposition reactor by the catalytic decomposition of xylene hydrocarbons at about 675 °C using ferrocene as a catalyst.[25] The PP was an amorphous resin (Grade 6331 Montell Polyolefins), having at 190 °C a viscosity of about 3000 Pa s. Composites containing mass fractions $x_m=0.005$, $x_m=0.01$, and $x_m=0.025$ of CNTs in PP were formed via melt blending using a twin-screw extruder.[24] The distribution of CNTs in the samples was examined by a laser scanning confocal microscope (model LSM510, Carl Zeiss, Inc.). Relatively uniform dispersions of CNTs (Fig. 1) were achieved without utilizing surfactants or surface functionalization of the tubes. Figure 1 shows that the dispersions consist of a relatively wide range of diameters and lengths of nanotubes. Although the initial length to diameter ratio of CNTs was $\approx$1000 before processing, the tubes fragment during mixing, which decreases the aspect ratio value after mixing.[23] The typical length of CNTs is on the order of 10 μm and the diameter is about 50 nm.[23,24] This polydispersity in CNT structure is typical of polymer nanocomposites formed with both single-wall and multiwall CNT materials due to the intrinsic disorder arising in the large scale fabrication process, the tendency of the CNT materials to form bundled structures, and the disorder introduced in the CNT later through the dispersion process.

The rheodielectric experiments were performed utilizing a standard rotational rheometer that was modified for the electrical characterization. The experiments were conducted at 190 °C under N_2 atmosphere using parallel circular plates separated by a gap (d) of about 0.80 mm. For a given rota-

FIG. 2. Test fixture. The surface of the shearing disk consists of alternating nonconductive (polyimide) and conductive (aluminum) electrode rings (r1, r2, and r3) to improve accuracy of the shear-rate measurement.

tional rate of the lower plate, the shear rate ($\dot{\gamma}$) increased radially as a function of position, so that conductivity measurements over the entire sample yielded an averaged value. Therefore, we utilized a custom-made test cell constructed from three conductive aluminum rings (r_1, r_2, and r_3) (Fig. 2) of width w separated by nonconductive polyamide regions. This configuration allowed us to measure the conductivity at well-defined shear rates and better observe possible transitions. At moderate shear rates ($1\ s^{-1} > \dot{\gamma} \geq 0.2\ s^{-1}$), the conductivity from the three rings collapsed onto a single curve when plotted versus the actual shear rate at each ring (data not shown).

Complex impedance measurements (impedance magnitude $|Z^*|$ and the corresponding phase angle θ) of our CNT-PP composites were conducted in the frequency range of 40 Hz to 1 MHz through a four-terminal technique using an Agilent 4294A precision impedance analyzer, calibrated with a standard extension adapter to short, load, and open standards. The complex conductivity, $\sigma^* = \sigma' + j\sigma''$, was obtained from the measured complex impedance Z^* normalized by the geometry of the test fixture,

$$\sigma^* = \frac{d}{Z^*(r \times w)}, \tag{1}$$

where d is the sample thickness, and the product of r and w represents area of the ring electrode. These conductivity measurements were made in the *shear gradient* direction, i.e., perpendicular to flow streamlines.

The distinctive feature of the dielectric limit is $\sigma' \approx 0$, and a linear dependence of the imaginary conductivity (σ'') with frequency, while $\theta \approx -90°$. The lowest measurable conductivity in our system was $|\sigma^*| = |\sigma''| = 5 \times 10^{-9}$ S/m at 40 Hz, which is illustrated in Fig. 3(b) [plot (8)], for an air gap when the sample was removed. The upper measurement limit of

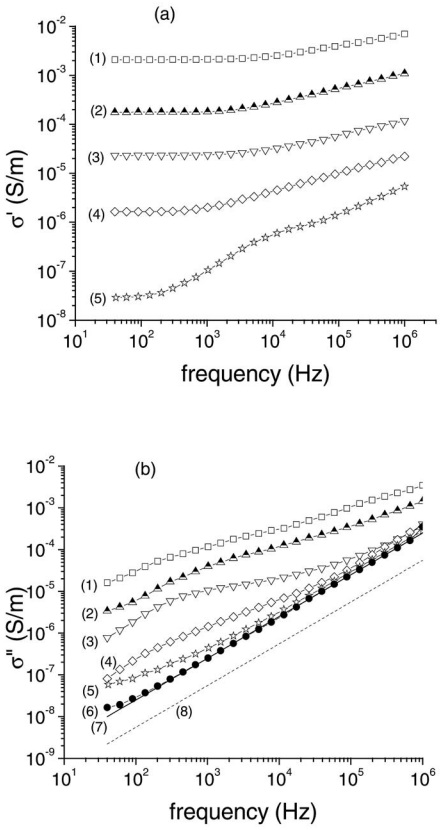

FIG. 3. (a) Real part σ' and (b) imaginary part σ'' of complex conductivity as a function of frequency for $x_m = 0.005$ CNT in PP measured at the following shear rates: (1) $10^{-3}\ s^{-1}$, (2) $0.2\ s^{-1}$, (3) $0.6\ s^{-1}$, (4) $1.0\ s^{-1}$, (5) $1.6\ s^{-1}$, (6) $3.0\ s^{-1}$, and (7) $6.3\ s^{-1}$. (8) Conductivity of an air gap when the sample was removed.

the real conductivity was verified by bringing the two plates of the test fixture into contact in the absence of a sample, which resulted in $|Z^*|$ of $1 \pm 0.1\ \Omega$ and $\theta = (0 \pm 0.2)°$. For lossless dielectric materials, θ is characteristically near $-90°$, while in the case of dielectrics with a loss due to intrinsic real conductivity, the phase angle between the ac voltage and the resulting current is in the range of $-90° \leq \theta < 0°$. The combined relative experimental uncertainty of the measured complex conductivity magnitude was within 2%, while the experimental uncertainty of the dielectric phase angle measurements was about ±0.5°.

RESULTS

In Figs. 3 and 4, we examine the frequency dependent complex conductivity results as a function of shear rate at 190 °C for the $x_m = 0.005$ and $x_m = 0.025$ formulations. The real part (σ') of the complex conductivity exhibits a plateau that extends up to a certain frequency ω_s. Throughout this paper, we denote the frequency independent real conductivity $\sigma'(\omega \to 0, \theta \approx 0)$ as σ_0. Our highest σ_0 values are in the range of about 0.01 S/m [Fig. 4(a), plot (1)], an order of magnitude larger than has been previously reported for similar composites.[22] At higher frequencies, $\omega > \omega_s$, σ' increases with increasing frequency according to the power law, σ'

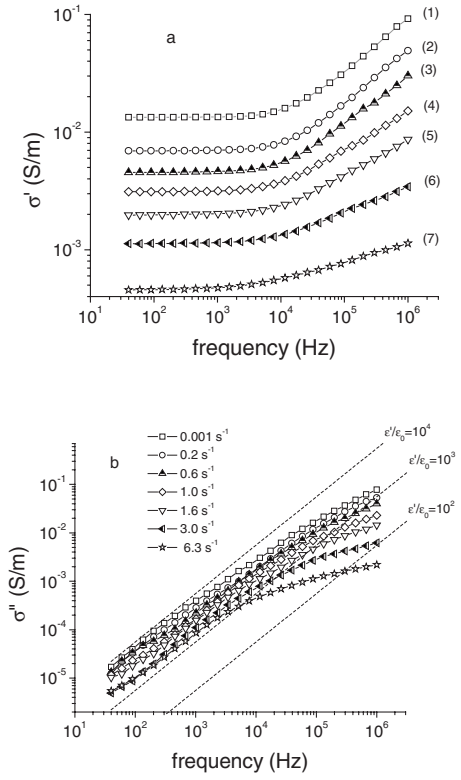

FIG. 4. (a) Real part σ' and (b) imaginary part σ'' of complex conductivity as a function of frequency for $x_m=0.025$ CNT in PP measured at the following shear rates: (1) 10^{-3} s^{-1}, (2) 0.2 s^{-1}, (3) 0.6 s^{-1}, (4) 1.0 s^{-1}, (5) 1.6 s^{-1}, (6) 3.0 s^{-1}, and (7) 6.3 s^{-1}.

$\sim \omega^n$, which is commonly described as a universal transport property of disordered solids and applicable to a broad range of semiconducting materials, conductor-dielectric mixtures, and composites.[26–29] The power law exponent (n) is positive and less than 1 and, in our measurements, found to be about 0.4. The dipolar and carrier polarization, expressed by the real part of the dielectric permittivity (ε_r'), contribute primarily to σ''. The complex conductivity response of conductor-dielectric mixtures, such as CNT-PP, is often analyzed in terms of the resistance-capacitance (R-C) *percolation model*, in which the conducting and dielectric properties of the mixture are represented by a network of idealized resistors and capacitors.[28–30] In the investigated frequency range, it is convenient to represent the equivalent circuit of such a network in terms of lumped capacitance (C) connected in parallel with a resistance (R). The equivalent complex admittance is the sum of the admittances of these two elements.[30–33] The complex conductivity σ^* of a specimen having thickness (d) and the active area of electrodes ($A=rw$) can be expressed by Eqs. (2a)–(2c)

$$\sigma^* = \sigma_0 + j\omega\varepsilon_0\varepsilon_r^*, \tag{2a}$$

where $\omega=2\pi f$ is again the angular frequency, ε_r^* is the complex relative dielectric permittivity of the material, $\varepsilon_r^*=\varepsilon_r' - j\varepsilon_r''$, ε_0 is the dielectric permittivity of free space, and $j^2=-1$. Separating Eq. (2a) into real and imaginary components, we obtain

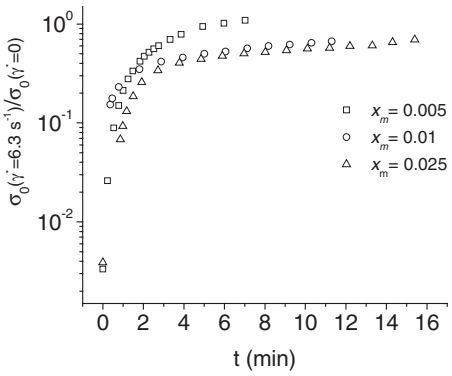

FIG. 5. Conductivity recovery in time upon the cessation of shear from $\dot{\gamma}=6.3$ s^{-1}.

$$\sigma' = \sigma_0 + \omega\varepsilon_0\varepsilon_r'' \tag{2b}$$

and

$$\sigma'' = j\omega\varepsilon_0\varepsilon_r'. \tag{2c}$$

Thus, scaling with frequency of the in-phase component of the complex conductivity (σ') depends on the frequency dependence of $\varepsilon_r''(\omega)$, while the corresponding dielectric dispersion of $\varepsilon_r'(\omega)$ determines scaling of σ'' with frequency. We determined σ_0 values by fitting the experimental σ' data to Eq. (2b) using a nonlinear least-squares fitting routine.

The imaginary part σ'' of the complex conductivity is shown in Figs. 3(b) and 4(b), where the slope of the plots corresponds to the real part (ε_r') of the complex dielectric permittivity [Eq. (2c)]. The dashed straight lines represent σ'' calculated as a reference for several constant values of ε_r'. It is seen in Figs. 3(b) and 4(b) that the measured σ'' deviates from linearity, especially at higher frequencies, indicating that the composites exhibit not only the frequency dependent conduction but also a frequency dependent dielectric polarization and dispersion. Depending on the CNT concentration and shear rate, ε_r' can change by several orders of magnitude. In the case of large CNT concentration ($x_m=0.025$) and small shear rates, ε_r' approaches a value of about 10^4 [Fig. 4(b), plot (1)]. With decreasing CNT concentration and increasing shear rate, ε_r' decreases to about 10^2 [Fig. 3(b), plot (1)] and eventually approaches the dielectric limit of the polymer matrix (PP), about 4.5 [see Fig. 3(b), plot (6)].

Figure 5 illustrates the time dependence of σ_0 at isothermal conditions of 190 °C after shearing was stopped. For each of the compositions considered, σ_0 returns to its near quiescent value. A 60% σ recovery for $x_m=0.005$, 0.01, and 0.025 nanocomposites occurred after about 3, 9, and 14 min, respectively. A similar recovery effect has been reported for PP-CNT melts extruded at 220 °C.[23] The conductivity recovery was attributed to the reorganization of the percolation network and the reformation of the local contacts between the nanotubes and to the reorientation of nanotubes oriented in the shear flow.[22]

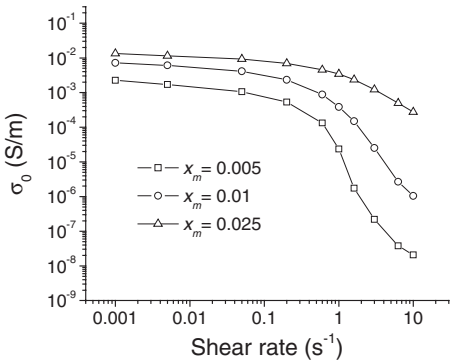

FIG. 6. Conductivity σ_0 as a function of shear rate.

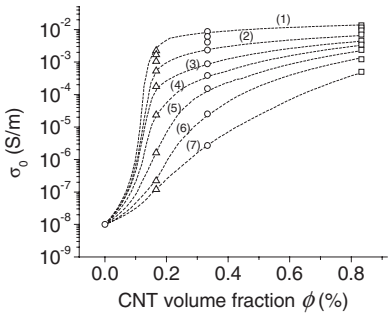

FIG. 7. Conductivity as a function of CNT concentration. The lines represent the GEM percolation model and are plotted for guiding the eyes at the following shear rates: (1) 10^{-3} s^{-1}, (2) 0.2 s^{-1}, (3) 0.6 s^{-1}, (4) 1.0 s^{-1}, (5) 1.6 s^{-1}, (6) 3.0 s^{-1}, and (7) 6.3 s^{-1}.

DISCUSSION

Effect of shear on the conductivity percolation concentration

The enhanced conductivity (σ_0) of polymer materials through the addition of CNT is currently one of the few commercially viable applications of these additives[1–3] and, therefore, we focus on this property and how it is modified under shear conditions. Figure 6 illustrates the effect of shear on σ_0 for all three compositions. At low shear rates, the conductivity decreases slightly with increasing $\dot{\gamma}$ as noted previously,[9] whereas above a critical value, it falls precipitously. Evidently, a lower concentration CNT dispersion is substantially more susceptible to perturbation by flow. The overall character of the conductivity plots suggests a *reverse-percolation* transition where higher $\dot{\gamma}$ would correspond to a lower concentration of the conducting filler. In the case of x_m=0.005, σ_0 approaches the insulating limit of the PP matrix of about 10^{-8} S/m at $\dot{\gamma}$ above 6 s^{-1}. At these high shear rates, the conductivity data almost coincide with pure PP, indicating that the material becomes a shear-induced dielectric insulator. This sensitivity of σ_0 to flow in the percolated CNT network is illustrated in Fig. 7. For the quiescent case, we find that the characteristic steep rise in conductivity starts at a volume fraction of about 0.0012 ($x_m \approx 0.0036$). The applied shear field shifts the percolation condition for σ_0 to higher CNT content and shear also broadens the transition. These observations confirm our hypothesis that the sensitivity of the CNT network to an applied shear flow perturbation is greatest at the beginning of the percolation transition where CNT only forms a *weakly* interconnected network. The network becomes more robust when the CNT concentration is several times above the percolation threshold.

According to the classical effective medium theory of Bruggeman,[34] the conductivity (σ_0) of a mixture is given by an average between the conductivities of the insulating matrix (σ_m) and the conductivity of the pure additive material (σ_a),

$$(1-\phi)\frac{\sigma_m-\sigma_0}{\sigma_m+2\sigma_0}+\phi\frac{\sigma_a-\sigma_0}{\sigma_a+2\sigma_0}=0, \tag{3}$$

where ϕ is the volume fraction of the conducting phase and where the matrix is a relatively insulating material. By construction, effective medium theory recovers the exact result of Maxwell[16] and Torquato[17] for the low concentration limit where a simple virial expansion applies. Scaling arguments based on percolation theory, where the conductivity of the matrix is entirely neglected and the particles are taken to be infinitely conductive, imply that σ_0 exhibits the scaling form

$$\sigma_0=\sigma_m[\phi_c/(\phi_c-\phi)]^s, \quad \phi<\phi_c \tag{4a}$$

and

$$\sigma_0=\sigma_a[(\phi-\phi_c)/(1-\phi)]^t, \quad \phi>\phi_c, \tag{4b}$$

where ϕ is the CNT volume fraction, ϕ_c is the critical percolation concentration, and s and t are "critical exponents" defined by the lattice percolation theory. The GEM model[19,25,33] formally "merges" the percolation and effective medium theories. In particular, this theory indicates that σ_0 is the following function of the conductivities of constituents:

$$(1-\phi)\frac{\sigma_m^{1/s}-\sigma_0^{1/s}}{\sigma_m^{1/s}+A\sigma_0^{1/s}}+\phi\frac{\sigma_a^{1/t}-\sigma_0^{1/t}}{\sigma_a^{1/s}+A\sigma_0^{1/t}}=0, \tag{5}$$

where A is a parameter related to the percolation concentration $A=(1-\phi_c)/\phi_c$. This extension of Eq. (3) recovers Eqs. (4a) and (4b), the scaling behavior for ϕ near ϕ_c by construction. The shortcoming of this procedure is that the exact perturbative result of Maxwell[16] and Torquato[17] is no longer recovered in the dilute limit since σ_0 is no longer analytic in the additive concentration. Despite this problem, GEM provides a significant improvement over the percolation theory since it interpolates between the low and high concentration additive regimes, while at the same time exhibiting a critical scaling behavior near the conductivity percolation threshold where σ_0 varies rapidly.

We seek to determine the conductivity percolation concentration (ϕ_c) as a function of shear rate by analyzing the data shown in Fig. 6 in terms of Eq. (5), which we solve for ϕ_c using a nonlinear least-squares routine. In fitting to the GEM relation, Eq. (5), the volume fraction (ϕ) of CNTs in PP was determined assuming a typical density of the CNTs of about 2.6 g/cm^3 (Ref. 35) and a PP density of about 0.78 g/cm^3. Based on these estimates, the volume fraction of nanotubes is found to be about 0.3 times the mass fraction. From the sigmoidal character of the experimental data plotted in Fig. 6, we determine the parameters in Eq. (5). The

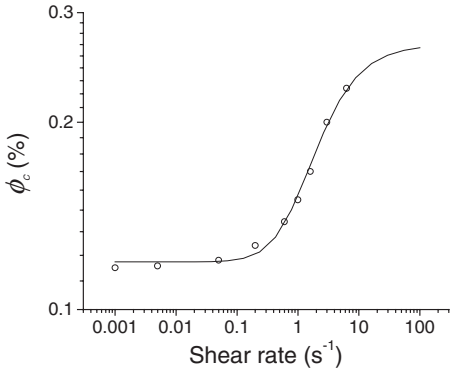

FIG. 8. Critical percolation concentration (ϕ_c) as a function of shear rate where symbols represent the calculated ϕ_c data, while the solid line is a fit to Eq. (3).

conductivity of the PP matrix was determined to be σ_m (PP) $\approx 10^{-8}$ S/m (Fig. 6) and the conductivity of the CNT material σ_A (CNT) was estimated to be on the order of 10^{-2} S/m for low shear rates and 10^{-3} S/m for high shear rates. The conductivity of the composite in the high CNT concentration limit is evidently not equivalent to that of an isolated tube. At high concentrations, the CNTs form a porous networklike structure rather than a continuous solid (see Fig. 1). σ_A (CNT) also depends on $\dot{\gamma}$ since shear influences the contact distribution and presumably the contact resistance between the CNT, effects that are not really addressed in the simple GEM model. As previously observed for the GEM model, especially for CNT materials,[36] the fitted values of the exponents do not conform exactly to the lattice percolation theory, which is certainly understandable given the approximations involved. We were able to fix the exponent t governing the concentration dependence of σ_0 in the low shear-rate regime to the theoretically expected value of $t=2$ (Refs. 37 and 38) for all our data, but the value of the other exponent s had to be adjusted ($s \approx 1.3-2.7$) compared to the theoretically expected value of $s=0.7$.[37,38] This difficulty is almost certainly due to the fact that the GEM theory relies on an effective medium theory for spherical particles as its basis in Eqs. (4a) and (4b), while the CNT clearly does not conform to this approximation. In particular, the virial coefficient $[\sigma]$ is exactly 3 from the work of Maxwell for particles much more conductive than the polymer matrix,[16] while this quantity is predicted to be on the order of 10^3 for particles having an aspect ratio on the order of those in our CNT samples.[17] Much of this effect can be adsorbed into the fitting of the percolation concentration to experiment, but this procedure clearly has its limitations for particles as anisotropic as the CNT.

The functional dependence of the GEM model for σ_0 provides a satisfactory description of the conductivity change with CNT concentration that we observed (Fig. 7). The resulting estimates of ϕ_c as a function shear rate are shown in Fig. 8. For the quiescent case, we find that the ϕ_c is on the order of 0.12% volume fraction, while the applied shear field monotonically shifts ϕ_c to a higher CNT concentration. Application of shear also induces an overall *broadening* of the insulator-conductor transition as a function of CNT concentration. These two effects are particularly evident at larger shear rates. For example, the conductivity percolation concentration transition at $\dot{\gamma}=6.3\ s^{-1}$ is shifted to about $\phi_c \approx 0.24\%$ volume fraction, which is approximately *twice* its quiescent value. This trend is predicted by the geometrical percolation theory under the reasonable assumption that shear causes some alignment of the CNT, which is known to increase the geometrical percolation threshold in networks formed of overlapping extended particles.[39,40]

The influence of shear on the viscosity of dispersions of extended particles in fluids has been considered in several previous works and the shear dependence of the viscosity percolation threshold analog of ϕ_c was estimated in this context.[41] The application of shear to such an inhomogeneous fluid induces stresses on the particles, which in turn induce long-range dipolar elastic fields in the fluid that react back upon the applied shear fields at the boundaries of fluid dispersion. This problem is mathematically analogous, at low particle concentrations, to calculating the conductivity change of a suspension of highly conducting particles in a relatively insulating fluid.[42–44] Basically, this connection arises because the fluid shear viscosity η is simply proportional to the momentum diffusion coefficient of the fluid so that $1/\eta$ is the momentum conductivity or "fluidity".[45] Thus, we may utilize here the viscosity percolation threshold estimates to describe the shear-rate dependence of ϕ_c,[41]

$$\phi_c(\dot{\gamma}) = \phi_{co} + (\phi_{c\,\max} - \phi_{co})\frac{(\tau\dot{\gamma})^2}{1+(\tau\dot{\gamma})^2}. \tag{6}$$

In Eq. (6), ϕ_{co} is the quiescent value of ϕ_c, the amplitude $\phi_{c\,\max} - \phi_{co} = \Delta\phi_c$ is the maximum change in ϕ_c induced by the flow, and τ is a flow relaxation time governing the flow-induced particle orientation process, which has been suggested[39] to be on the order of the structural relaxation time of an entangled polymer melt matrix. Specifically, the anisotropic particles are assumed to be dispersed isotropically for $\dot{\gamma} \to 0$ and the shift $\phi_{c\,\max} - \phi_{co}$ describes the effect of particle alignment along the shear field direction in the limit $\dot{\gamma} \to \infty$. Figure 8 shows a fit of the ϕ_c data to Eq. (6), where we obtain $\tau \approx 1$ s. The observation that ϕ_c increases with $\dot{\gamma}$ according to Eq. (6) supports our interpretation of the conductor-insulator transition as arising from the partial flow-induced alignment of the CNTs along the fluid flow direction.[25] The maximum change in $\Delta\phi_c$ occurs for $\dot{\gamma}_c \approx 1/\tau \approx 1\ s^{-1}$, which is consistent with τ being comparable to the structural relaxation time of the polymer matrix (see Fig. 3 of Ref. 7). The emergence of a highly conducting state from the mutual collective interactions of the CNTs means that it is naive to visualize these changes in terms of the orientation of individual isolated tubes. A large part of this trend must also reflect the breaking down of the CNT network structure that forms through a combination of direct intertube attractive interactions, topological interactions between the tubes due to strong excluded volume interactions that keep the tubes from passing through each other under flow and strong direct contact interactions arising from the physical impingement of these relatively rigid particles. In

our previous work,[7] we explained the shear-induced changes in the viscoelastic properties in terms of these same factors.

Conductivity recovery upon succession of shear

Now that we have established the strong effect of shear on σ_0 for concentrations near, but above, ϕ_c, we examine the ability of these nanocomposites to recover their electrical characteristics upon the *cessation* of shear. While we might expect that the nanotubes should remain "frozen" in place once the flow stops (due to the non-Brownian nature of the annotate mobility within the polymer matrix), we actually found that the conductivity was recoverable. Indeed, Fig. 5 illustrates that at each of the compositions considered, σ_0 returns to its near quiescent value. A 60% σ recovery for $x_m=0.005$, 0.01, and 0.025 nanocomposites occurred after about 3, 9, and 14 min, respectively. We note that Huang *et al.*[46] have recently made a study of the viscoelastic properties of CNTs in viscous polymer matrices, where substantial variations of the dispersion properties in relation to mixing time and where very large changes in the shear viscosity were noted when the melt composites were left to stand over the time scales of weeks. These variations were attributed to the "reaggregation" of the CNTs, despite the non-Brownian conditions of these observations. The data in Fig. 5 serve to quantify this type of "aging" phenomenon in a system where the kinetics is more amenable to quantitative study. In future work, we plan to consider the influence of temperature and concentration on this technologically important phenomenon.

Since Brownian motion should not be effectively operative in leading to relaxation in these sheared dispersions, we need to consider other mechanisms that could drive the relaxation process. The deformation of the tubes under flow in a polymer melt[47] provides a clear candidate for this effect, and we suggest that the relaxation is driven by the residual stresses in the CNT dispersed melt that are induced under steady flow conditions. This hypothesis could be checked by Raman or other scattering techniques that are sensitive to stress effects on the tubes.[48–50] In a recent work, it has been suggested that CNTs can inhibit the relaxation of the large residual stresses that accompany the formation of semicrystalline polymer materials, thereby affecting the brittleness of the resulting solidified material.[51] Recent work has suggested that the presence of unstable mechanically strained filler in a stable elastic matrix can lead to materials with extreme mechanical damping characteristics.[52,53] CNT-polymer nanocomposites seem to be very promising for fabricating such materials by simply quenching the CNT filled melt into a solidified state after a flow. It seems clear that future work should better quantify the effect of residual stress effects in polymer nanocomposites and their effect on the mechanical and dielectric properties of polymer nanocomposite materials and the evolution of these properties over long time scales.

Conductivity scaling with frequency

The measured ac conductivity response of the *double network* of carbon nanotubes interpenetrating an entangled PP polymer matrix above percolation can be described by a random impedance network model with hopping transport of charge carriers, in which conductivity and dielectric properties are represented by a network of resistors (R) and capacitors (C).[28–30] Typical dielectric loss data for CNT-PP extracted from the ac conductivity data $[\varepsilon_r''\varepsilon_0=(\sigma'-\sigma_0)/\omega]$ are shown as a function of frequency in Fig. 9 for $x_m=0.025$. There is a broad loss peak in each plot. This loss peak is characteristic when the charge transport is due to multidimensional variable range hopping.[28,29,54]

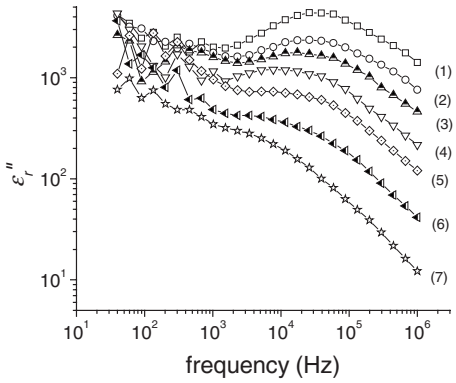

FIG. 9. Imaginary part of the dielectric permittivity for $x_m=0.025$ as a function of frequency at the following shear rates: (1) 10^{-3} s^{-1}, (2) 0.2 s^{-1}, (3) 0.6 s^{-1}, (4) 1.0 s^{-1}, (5) 1.6 s^{-1}, (6) 3.0 s^{-1}, and (7) 6.3 s^{-1}.

The crossover frequency ω_s corresponds to the macroscopic relaxation frequency ω_τ and it is defined by the peak frequency of the dielectric loss. These features reflect hopping conduction in disordered media.[29,54] The shoulder that develops with increasing shear rate in the percolation regime at $\omega<\omega_s$ indicates that the dimensionality of the system decreases with shearing, consistent with the flow-induced alignment of the CNTs discussed earlier. Above ω_s, in the multiple hopping regime, $\omega_s<\omega<\omega_0$, where ω_0 is the microscopic cutoff frequency, conduction occurs in the isolated clusters of sites and the real part of the conductivity increases with ω.

There has been a long debate in the literature regarding how to determine the crossover frequency of the onset ac conductivity for the master plot. The proposed procedures are often based on somewhat arbitrary assumptions.[4,32,35] For example, ω_s has been defined as a frequency when $\sigma'(\omega_s)/\sigma_0=10^{0.5}$ (Ref. 52) or that $\sigma'(\omega_s)/\sigma_0=1.1$ at ω/ω_s,[4] or a simple representative conductivity plot selected as a scaling reference.[55] Although the crossover frequency is the microscopic relaxation frequency, it is difficult to quantitatively analyze the dielectric relaxation spectrum (Fig. 9) in the presence of a charge transport that is governed by the statistic of the dominant hopping sites and yet coupled with polarization effects due to disorder. According to the percolation conductivity model,[36,54,55] the macroscopic crossover frequency depends on the percolation critical exponents and the critical volume fraction: $\omega_s=\omega_0|\phi-\phi_c|^{(s+t)}$. Since in our analysis percolation parameters are related to σ_0, we find that ω_s/ω_0 indeed scales linearly with σ_0.[32] On the other hand, ω_s depends on the nature of distribution of the hopping conductivity sites in disordered materials, i.e., reflects the resis-

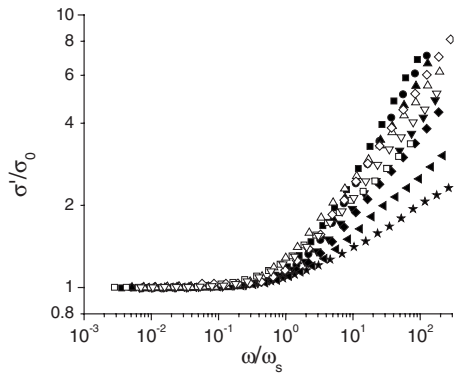

FIG. 10. Scaled conductivity (σ'/σ_0) vs scaled frequency (ω/ω_s) for $x_m=0.01$ (open symbols) and $x_m=0.025$ (closed symbols) at different shear rates: 10^{-3} s^{-1} (squares), 0.2 s^{-1} (circles), 0.6 s^{-1} (triangles—up), 1.0 s^{-1} (triangles—down), 1.6 s^{-1} (diamonds), 3.0 s^{-1} (tilt triangles), and 6.3 s^{-1} (stars).

tance between hopping sites and effective capacitance and, therefore, it should accordingly scale with the dielectric permittivity.[35,54,55] Hence, we can assume equivalence between ω_s and the macroscopic relaxation frequency (ω_τ),

$$\omega_\tau = \omega_s = \sigma_0/(\varepsilon_0|\varepsilon_r^*|)_{\omega_\tau}. \tag{7}$$

We observed that ω_s increases with increasing σ_0, while it decreases when the dielectric permittivity increases, $\omega_s \approx \sigma_0/(\varepsilon_0|\varepsilon_r^*|) \approx \omega_\tau$. These two opposite trends are illustrated in Figs. 3 and 4. For example, $\omega_s/2\pi$ is about 27 kHz in Fig. 3(a) [plot (1)], σ_0 is about 2.0×10^{-3} S/m, and $|\varepsilon_r^*|$ is about 1.4×10^3. In comparison, $\omega_s/2\pi$ decreases to about 13.6 kHz in Fig. 4(a) [plot (5)], where $|\varepsilon_r^*|$ is about 2.6×10^3 at a similar σ_0 value of about 1.97×10^{-3} S/m.

Figure 10 shows the results of scaled $\sigma'(\omega)/\sigma_0$ according to Ref. 54 with ω_s obtained by solving iteratively Eq. (7) against $\varepsilon_r'(\omega)$ and $\varepsilon_r''(\omega)$. The scaled conductivity for $\phi > \phi_c$ compares well with the universal trend showing a power law behavior $(\sigma' \sim \omega^n)$ at $\omega > \omega_s$. The plateau in the conductivity at $\omega < \omega_s$ indicates the existence of one or more percolation paths of the resistive elements across the network that comprise an infinite cluster. The value of n in Fig. 10 is about 0.4 for all $\phi_c < 0.13\%$. At higher ϕ_c, the exponent n decreases continuously with increasing ϕ_c, approaching a value of about 0.12 at ϕ_c of about 0.23% volume fraction. The decreasing value of n indicates that the fraction of resistive paths decreases with shearing in favor of the developing network of insulating capacitance elements (C),[26,28,30] consistent with the shear-induced conductor-insulator transitions.

CONCLUSION

The blending of carbon nanotubes into polymer matrices leads to composite materials whose properties can depend strongly on the flow history to which the materials have been subjected. Through ac conductivity measurements, we observed the *conductor-insulator* or "percolation" transition in melt-mixed dispersions of multiwall CNTs in polypropylene over a narrow range of CNT concentrations. The shear-induced conductor-insulator transition has its origin in the shear-rate dependence of the critical percolation concentration (ϕ_c), which increases with shear rate in accordance with our model for the shear-dependent percolation threshold. According to this model, the quiescent value of ϕ_c is on the order of 0.12% volume fraction (0.36% mass fraction), while the structural relaxation time of the polymer matrix is about $\tau \approx 1$ s. The observation that ϕ_c increases with $\dot{\gamma}$ according to Eq. (6) indicates that the $\dot{\gamma}$ field-induced alignment of the CNTs is along the fluid flow directions. Since ϕ_c and τ are universal parameters of the percolated network, Eq. (6) can be used as a predictive tool in the analysis of shear-induced behavior of other materials.

The character of the dielectric loss peak extracted from the complex conductivity data indicates that the charge transport is due to the multidimensional variable range hopping and that the dimensionality of the system decreases with shearing, consistent with the CNT alignment discussed earlier. In the quiescent regime, the frequency dependence of the real part of conductivity follows a "universal" power law scaling relation seen in many disordered materials.

Interestingly, under sufficiently high shear rates, the conducting composite becomes a shear-induced insulator. The conductivity of these nonequilibrium materials fully recovers upon cessation of flow. The results suggest that the presence of carbon nanotubes structures in a stable elastic matrix (PP) can lead to materials with interesting mechanical damping characteristics.

ACKNOWLEDGMENTS

We gratefully thank Eric Grulke for supplying the carbon nanotube composites and Erik Hobbie for important discussions.

*Corresponding authors.
†jan.obrzut@nist.gov
‡jack.douglas@nist.gov

[1] J. N. Coleman, S. Curran, A. B. Dalton, A. P. Davey, B. McCarthy, W. Blau, and R. C. Barklie, Phys. Rev. B **58**, R7492 (1998).
[2] R. H. Baughman, A. A. Zakhidov, and W. A. de Heer, Science **297**, 787 (2002).
[3] S. Barrau, P. Demont, A. Peigney, C. Laurent, and C. Lacabanne, Macromolecules **36**, 5187 (2003).
[4] B. E. Kilbride and J. N. Coleman, J. Appl. Phys. **92**, 4024 (2002).
[5] J. K. W. Sandler, J. E. Kirk, I. A. Kinloch, M. S. P. Shaffer, and A. H. Windle, Polymer **44**, 5893 (2003).
[6] F. M. Du, R. C. Scogna, W. Zhou, S. Brand, J. E. Fischer, and K. I. Winey, Macromolecules **37**, 9048 (2004).

[7] S. B. Kharchenko, J. F. Douglas, J. Obrzut, E. A. Grulke, and K. B. Migler, Nat. Mater. **3**, 564 (2004).
[8] M. J. Biercuk, M. C. Llaguno, M. Radosavljevic, J. K. Hyun, A. T. Johnson, and J. E. Fischer, Appl. Phys. Lett. **80**, 2767 (2002).
[9] M. B. Bryning, D. E. Milkie, M. F. Islam, J. M. Kikkawa, and A. G. Yodh, Appl. Phys. Lett. **87**, 161909 (2005).
[10] S. T. Huxtable, D. G. Cahill, S. Shenogin, L. P. Xue, R. Ozisik, P. Barone, M. Usrey, M. S. Strano, G. Siddons, M. Shim, and P. Keblinski, Nat. Mater. **2**, 731 (2003).
[11] P. Potschke, T. D. Fornes, and D. R. Paul, Polymer **43**, 3247 (2002).
[12] J. Suhr, N. Koratkar, P. Keblinski, and P. Ajayan, Nat. Mater. **4**, 134 (2005).
[13] Q. Zhao, M. D. Frogley, and H. D. Wagner, Polym. Adv. Technol. **13**, 759 (2002).
[14] J. R. Wood, Qing Zhao, M. D. Frogley, E. R. Meurs, A. D. Prins, T. Peijs, D. J. Dunstan, and H. D. Wagner, Phys. Rev. B **62**, 7571 (2000).
[15] P. Potschke, S. M. Dudkin, and I. Alig, Polymer **44**, 5023 (2003).
[16] J. C. Maxwell, *A Treatise on Electricity and Magnetism* (Dover, New York, 1954).
[17] S. Torquato, *Random Heterogeneous Materials: Micro-structure and Macroscopic Properties* (Springer-Verlag, New York, 2002).
[18] P. G. DeGennes, *Scaling Concepts in Polymer Physics* (Cornell University Press, Ithaca, NY, 1979).
[19] D. S. McLachlan, M. Blaszkiewicz, and R. E. Newnham, J. Am. Ceram. Soc. **73**, 2187 (1990).
[20] C. Brosseau, J. Appl. Phys. **91**, 3197 (2002).
[21] Y. T. Sung, M. S. Han, J. W. Jung, H. S. Lee, C. K. Kum, J. Joo, and W. N. Kim, Polymer **47**, 4434 (2006).
[22] I. Alig, D. Lellinger, S. M. Dudkin, and P. Potschke, Polymer **48**, 1020 (2007).
[23] J. Hilding, E. A. Grulke, Z. G. Zhang, and F. Lockwood, J. Dispersion Sci. Technol. **24**, 1 (2003).
[24] T. Kashiwagi, E. Grulke, J. Hilding, K. Groth, R. Harris, K. Butler, J. Shields, S. Kharchenko, and J. Douglas, Polymer **45**, 4227 (2004).
[25] R. Andrews, D. Jacques, D. Qian, and E. C. Dickey, Carbon **39**, 1681 (2001).
[26] H. Botteger and V. V. Bryskin, *Hopping Conduction in Solids* (Verlagsgesselshaft, Weinheim, 1985), Chaps. 2 and 5.
[27] D. S. McLachlan, W. D. Heiss, C. Chiteme, and J. Wu, Phys. Rev. B **58**, 13558 (1998).
[28] J. C. Dyre and T. B. Shroder, Rev. Mod. Phys. **72**, 873 (2000).
[29] A. G. Hunt, Philos. Mag. B **81**, 875 (2001).
[30] J. P. Clerc, G. Giraud, J. M. Laugier, and J. M. Luck, Adv. Phys. **39**, 191 (1990).
[31] F. Kremer and A. Schonhals, in *Broadband Dielectric Spectroscopy* (Springer, Berlin, 2003), Chap. 2.
[32] A. K. Jonscher, Nature (London) **267**, 673 (1977).
[33] D. P. Almond and C. R. Bowen, Phys. Rev. Lett. **92**, 157601 (2004).
[34] D. A. G. Bruggeman, Ann. Phys. **24**, 636 (1935).
[35] B. Kim, J. Lee, and I. Yu, J. Appl. Phys. **94**, 6724 (2003).
[36] D. S. McLachlan, C. Chiteme, C. Park, K. E. Wise, S. E. Lowther, P. T. Lillehel, E. J. Siochi, and J. S. Harrison, J. Polym. Sci., Part B: Polym. Phys. **43**, 3273 (2005).
[37] J. P. Straley, Phys. Rev. B **15**, 5733 (1977).
[38] I. Balberg and S. Bozowski, Solid State Commun. **44**, 551 (1982).
[39] S. H. Munson-McGee, Phys. Rev. B **43**, 3331 (1991).
[40] M. Moniruzzaman and K. I. Winey, Macromolecules **36**, 5194 (2006).
[41] J. Bicerano, J. F. Douglas, and D. A. Brune, J. Macromol. Sci., Rev. Macromol. Chem. Phys. **C39**, 561 (1999).
[42] J. F. Douglas and E. J. Garboczi, Adv. Chem. Phys. **91**, 85 (1995).
[43] M. L. Mansfield, J. F. Douglas, and E. J. Garboczi, Phys. Rev. E **64**, 061401 (2001).
[44] M. L. Mansfield and J. F. Douglas, Condens. Matter Phys. **5**, 249 (2002).
[45] M. L. Mansfield, J. F. Douglas, S. Irfan, and E. Kang, Macromolecules **40**, 2575 (2007).
[46] Y. Y. Huang, S. V. Ahir, and E. M. Terentjev, Phys. Rev. B **73**, 125422 (2006).
[47] E. K. Hobbie, H. Wang, H. Kim, S. Lin-Gibson, and E. A. Grulke, Phys. Fluids **15**, 1196 (2003).
[48] H. Ko, Y. Pikus, C. Jiang, A. Jauss, O. Hollricher, and V. V. Tsukruk, Appl. Phys. Lett. **85**, 2598 (2004).
[49] P. Puech, H. Hubel, D. Dunstan, R. R. Bacsa, C. Laurent, and W. S. Bacsa, Phys. Rev. Lett. **93**, 095506 (2004).
[50] C. Jiang, H. Ko, and V. V. Tsukruk, Adv. Mater. (Weinheim, Ger.) **17**, 2127 (2005).
[51] D. Xu, Z. Wang, and J. F. Douglas, Macromolecules **40**, 1799 (2007).
[52] R. S. Lakes, Philos. Mag. Lett. **81**, 95 (2001).
[53] R. S. Lakes, T. Lee, A. Bersie, and Y. C. Wang, Nature (London) **410**, 565 (2001).
[54] W. F. Pasveer, P. A. Bobbert, and M. A. J. Michels, Phys. Rev. B **74**, 165209 (2006).
[55] P. Gonon and A. Boudefel, J. Appl. Phys. **99**, 024308 (2006).